Single-walled Carbon Nanotube Modelling Based on Cosserat Surface Theory

YU ZHANG [a*], CARLO SANSOUR [b], CHRIS BINGHAM [a]
[a] School of Engineering, University of Lincoln,
Lincoln, LN6 7TS, U.K.
[b] School of Civil Engineering, University of Nottingham,
Nottingham, NG7 2RD, U.K.
* yzhang@lincoln.ac.uk

Abstract: - This paper investigates the mechanical properties of single-walled carbon nanotubes (SWCNTs). To overcome the difficulties of spanning multi-scales from atomistic field to macroscopic space, the Cauchy-Born rule is applied to link the deformation of atom lattice vectors at the atomic level with the material deformation at a macro continuum level. SWCNTs are modelled as Cosserat surfaces, and a modified shell theory is adopted where a displacement field-independent rotation tensor is introduced, which describes the rotation of the inner structure of the surface, i.e. the micro-rotation. Empirical interatomic potentials are employed so that the force and modulus fields can be computed by the derivations of potential forms from the displacement and rotation fields. The method is used to predict the Young's modulus for SWCNTs, and it is shown that it is capable of providing comparable results with atomistic simulations, but with much lower computational overhead.

Key-Words: - Single-walled carbon nanotube, Cauchy-Born rule, Cosserat surface, Empirical interatomic potential.

1 Introduction

The discovery of carbon nano-tubes (CNTs) and their outstanding properties [1] has led to a revolution in nano-technology. However, maximizing their potential is impeded by the relatively high cost of experiments, which is often inflated by the corruption of useful measurements due to unexpected manual and handling errors. It is therefore extremely useful to develop theoretical tools for studying the mechanical properties of CNTs, with results being of particular interest to aerospace, biomedical engineering and many other sectors.

To apply continuum mechanics to CNTs, the Cauchy-Born rule is often used to link the atomistic field to the continuum environment that describes the relationship between the deformation of atom lattice vectors and the deformation of bulk vectors [2]. However, as described in [2], the Cauchy–Born rule is not directly applicable to CNTs because they can be considered as a curved surface, and the deformation gradient maps the deformed vector on the tangent space of the deformed curve, instead of the real chord vector that resides on the curve. Modifications have been therefore been posed for the standard Cauchy-Born rule [2-4], all based on the addition of higher order terms into the deformation gradient in order to better approximate the real curve. Specifically, they have traditionally been modelled as either linear elastic shells [5,6] or non-linear elastic shells [2,7] using continuum mechanics methods.

Here however, the paper now uses the standard Cauchy-Born rule to describe the strain at the tangent plane, and a modification is proposed by adding a displacement field-independent rotation tensor at each point of the surface. A single-walled carbon nanotube (SWCNT) can be considered as a two-dimensional manifold and can be solved with the Cosserat surface shell theory demonstrated in [8], where the rotation field is already at a micro-level. However, this Cosserat surface shell theory is based on constitutive laws from conventional continuum theory—here the constitutive laws derived from empirical interatomic potentials which describe the real interactions among atoms.

The first generation of Tersoff and Brenner potentials [9] has been extensively applied in the study of CNTs [2,10-12], and in [13] modifications were published that are considered as a second generation of Brenner potentials, which they claimed to be more accurate to model the real interatomic reactions of carbon bonds. This forms the basis for the use of the empirical interatomic potential forms in this paper.

2 Modelling Method

The primary underlying principle of the method considered here, is that the SWCNT is a two-dimensional manifold whose solution is obtained using Cosserat surface shell theory. The deformation can be described by a stretch tensor and a rotation tensor. Responding to external force, the surface deforms providing a force stress field and a couple stress field. To solve for these four fields and thereby describe the material mechanical properties, one needs to identify the correct potential forms that are applicable at an atomistic level for continuum formulations. Here then, empirical functions of potentials are adopted which are practical and appropriate to describe the total potential of the SWCNT accurately.

2.1 Cauchy-Born Rule

Consider $\boldsymbol{\Phi}$ as the deformation map when a space-filling continuum body $\Omega_0 \subset \mathbb{R}^3$ deforms to $\Omega_t \subset \mathbb{R}^3$, i.e. $\Omega_t = \boldsymbol{\Phi}(\Omega_0)$. Let $\boldsymbol{X}$ define a point in the body Ω_0, while $\boldsymbol{x}$ is its position Ω_t after deformation. Then we have relationship $\boldsymbol{x} = \boldsymbol{\Phi}(\boldsymbol{X})$. The deformation gradient $\boldsymbol{F}$ is defined as the derivative of the deformation map, means that it maps infinitesimal line elements from the deformed configuration to the reference configuration:

$$d\boldsymbol{x} = \boldsymbol{F} d\boldsymbol{X} \quad . \tag{1}$$

Using elasticity theory, under finite strains, the deformation of space-filling continuum is homogeneous at the atomistic scale. Thus, the space-filling continuum undergoes the same deformation as the atomic lattice vectors as established by the Cauchy-Born rule:

$$\boldsymbol{a} = \boldsymbol{F}\boldsymbol{A} \quad , \tag{2}$$

where $\boldsymbol{a}$ is the deformed lattice vector, and $\boldsymbol{A}$ is the undeformed lattice vector in continuum. Eq.(2) is, in essence, the Cauchy-Born rule which provides the link between atomistic and continuum deformations.

Due to the non-centrosymmetric hexagonal atomic structure of CNTs, it is essential to introduce an in-plane shift vector as a bridge between the two centrosymmetric sub-lattices, as described in Fig.1. Let $\hat{\boldsymbol{a}}_i$ (i=1,2) define the basis vectors of a centrosymmetric sub-lattice, and $\hat{\boldsymbol{B}}$ be the relative shift vector of two sub-lattices. To reach the required degrees of freedom, an additional kinematic variable is introduced, by describing the perturbation of the shift vector, donated by $\boldsymbol{\eta}$. The bond vectors $\boldsymbol{A}_i$ (i=1,2,3) after the perturbation are

$$\boldsymbol{A}_i = \boldsymbol{A}_{0i} + \boldsymbol{\eta} \quad , \tag{3}$$

where $\boldsymbol{A}_{0i}$ are the undeformed vectors. Let $\hat{\boldsymbol{P}} = \hat{\boldsymbol{B}} + \boldsymbol{\eta}$, then the bond vectors are

$$\boldsymbol{A}_1 = -\hat{\boldsymbol{a}}_2 + \hat{\boldsymbol{P}}\ ,\ \boldsymbol{A}_2 = \hat{\boldsymbol{P}} \text{ and } \boldsymbol{A}_3 = -\hat{\boldsymbol{a}}_1 + \hat{\boldsymbol{P}} \quad . \tag{4}$$

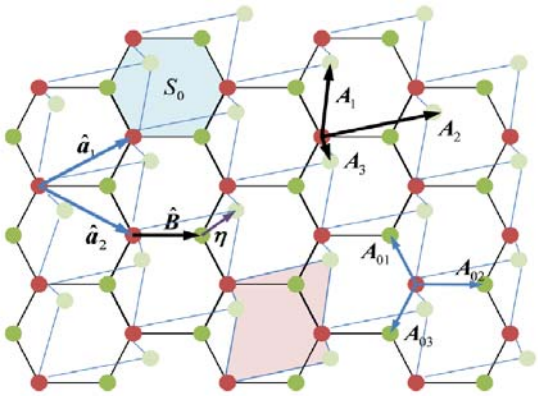

Fig. 1. Multi-lattice, sub-lattices, and shift vector

2.2 Cosserat Surface as a Shell Model

Let $\mathcal{B} \subset \mathbb{R}^3$ define a two-dimensional surface, and $\mathcal{B}_t$ is the surface at time *t*. At *t*, $\boldsymbol{X}$ is a point in the reference configuration, and x is the point in the deformed configuration, and the following relations hold

$$\boldsymbol{x}(t) = \boldsymbol{\varphi}(\boldsymbol{X}, t) \text{ and } \boldsymbol{X}(t) = \boldsymbol{\varphi}^{-1}(\boldsymbol{x}, t) \quad . \tag{5}$$

Notice, here $\boldsymbol{\varphi}$ is a surface to surface map. ϑ^α (α=1,2) are the co-ordinates attached to the surface at $\mathcal{B}$. Let $\mathcal{TB}$, $\mathcal{TB}_t$ be the tangent spaces of $\mathcal{B}$ and $\mathcal{B}_t$, respectively, and the covariant base vectors can be calculated as

$$\boldsymbol{G}_\alpha = \frac{\partial \boldsymbol{X}}{\partial \vartheta^\alpha} \text{ and } \boldsymbol{g}_\alpha = \frac{\partial \boldsymbol{x}}{\partial \vartheta^\alpha} \quad . \tag{6}$$

The deformation gradient is defined as the tangent of the surface map, $\boldsymbol{F} = \mathcal{T}\boldsymbol{\varphi}$. F can be give as tensor product

$$\boldsymbol{F} = \boldsymbol{g}^\alpha \otimes \boldsymbol{G}_\alpha \quad . \tag{7}$$

The displacement field is introduced by the displacement vector

$$\boldsymbol{u} = \boldsymbol{x} - \boldsymbol{X} \quad , \tag{8}$$

and we have

$$\boldsymbol{F} = (\boldsymbol{G}_\alpha + \boldsymbol{u}_{,\alpha}) \otimes \boldsymbol{G}_\alpha \ , \tag{9}$$

where comma denotes partial derivatives.

One of the assumptions of shell theory is that a displacement field, as well as a rotation field, are attached to the Cosserat surface, both of which are assumed to be independent of one another. The rotation field is introduced by an orthogonal tensor $\boldsymbol{R} \in \mathrm{SO}(3)$ which is defined as

$$\boldsymbol{R} = \exp(\boldsymbol{\Omega}) = 1 + \frac{\sin|\boldsymbol{\omega}|}{|\boldsymbol{\omega}|}\boldsymbol{\Omega} + \frac{1-\cos|\boldsymbol{\omega}|}{|\boldsymbol{\omega}|}\boldsymbol{\Omega}^2 \ , \tag{10}$$

And where $\boldsymbol{\Omega} = -\boldsymbol{\Omega}^T$ with $\boldsymbol{\omega}$ to be the corresponding axial vector of $\boldsymbol{\Omega}$.

Then, the first Cosserat deformation tensor is defined as

$$\boldsymbol{U} := \boldsymbol{R}^T \boldsymbol{F} \quad . \tag{11}$$

and the second Cosserat deformation tensor is

$$\boldsymbol{K} = -\frac{1}{2}\boldsymbol{\varepsilon} : \boldsymbol{R}^T \boldsymbol{R}_{,\alpha} \otimes \boldsymbol{G}^{\alpha} \, . \tag{12}$$

where $\boldsymbol{\varepsilon}$ is the Ricci tensor, and (**:**) denotes a double contraction.

Using pure 'mechanical theory', the internal potential function for the Cosserat surface depends on the two strain tensors $\boldsymbol{U}$ and $\boldsymbol{K}$

$$V_{\text{int}}(\boldsymbol{U}, \boldsymbol{K}) = \int_{\mathcal{B}} \rho \phi_{\text{int}}(\boldsymbol{U}, \boldsymbol{K}) dA \, , \tag{13}$$

where ρ is the density of the surface. The force tensor and the couple tensor are defined as

$$\boldsymbol{S} := \rho \frac{\partial \phi_{\text{int}}(\boldsymbol{U}, \boldsymbol{K})}{\partial \boldsymbol{U}} \text{ and } \boldsymbol{T} := \rho \frac{\partial \phi_{\text{int}}(\boldsymbol{U}, \boldsymbol{K})}{\partial \boldsymbol{K}} \, . \tag{14}$$

Notice that here $\boldsymbol{S}$ and $\boldsymbol{T}$ are the Boit-like stress tensors, which is different from but related with the first and second Piola-Kirchhoff stress tensor. For the Cosserat surface, the principle of virtual work holds

$$\delta V_{\text{int}}(\boldsymbol{U}, \boldsymbol{K}) - W_{ext} = 0 \quad . \tag{15}$$

where W_{ext} is the external virtual work. For further information, readers are directed to [8].

2.3 Potentials

The mechanical properties of CNTs are largely determined by the interatomic forces, which are governed by the chemical bonds, expressed in terms of interatomic potential models. In this paper, a second generation Brenner reactive empirical bond order (REBO) potential is chosen, where the total potential of the system is given by

$$V_{REBO} = \sum_i \sum_{j=i+1} \left[V_R(r_{ij}) - \bar{b}_{ij} V_A(r_{ij}) \right], \tag{16}$$

where r_{ij} is the distance between atoms *i* and *j*, and $\bar{b}_{ij}$ is many-body empirical bond order term. V_R and V_A are the repulsive and attractive terms, with

$$V_R(r) = f_c(r)\left(1 + \frac{Q}{r}\right) A \exp(-\alpha r) \quad ,$$

$$V_A(r) = f_c(r) \sum_{n=1}^{3} B_n e^{-\beta_n r} \, , \tag{17}$$

where f_c is a cut-off function.

The full expansion of the empirical potential form and the selections of the parameters are directed to [13] for further explanation. It can be seen that the potential form is a function of the bond lengths and the bond angles between two adjacent atoms and also with the second neighbourhood atoms.

3 SWCNT Modelling

Cosserat surface theory is applied in modelling and simulating SWCNTs' behaviour, when they are modelled as cylindrical shells. Empirical potential forms are applied. The in-plane and out-of-plane contributions are derived for the calculation of stress and moment fields.

If an atom *A* is considered to be the origin (*i* atom), the potential is expressed as $V = V(r_{ij}, r_{ik}, r_{jk}, \theta_{ijk}, \theta_{jik})$, which involves the atoms at atom *A*'s first neighbourhood and second neighborhood, as shown in Fig.2.

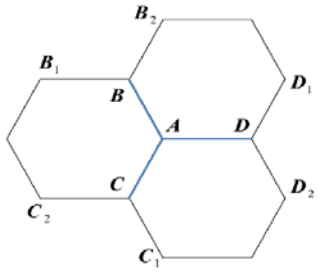

Fig. 2. Atom *A* and its first and second nearest neighbors

Defining

$$V_{AB} = V(r_{AB}, r_{AC}, r_{AD}, \theta_{BAC}, \theta_{BAD}),$$
$$V_{AC} = V(r_{AC}, r_{AB}, r_{AD}, \theta_{BAC}, \theta_{CAD}),$$
$$V_{AD} = V(r_{AD}, r_{AB}, r_{AC}, \theta_{BAD}, \theta_{CAD}),$$
$$V_{BA} = V(r_{BB_1}, r_{BB_2}, r_{BA}, \theta_{B_1BA}, \theta_{B_2BA}),$$
$$V_{CA} = V(r_{CC_1}, r_{CC_2}, r_{CA}, \theta_{C_1CA}, \theta_{C_2CA}),$$
$$V_{DA} = V(r_{DD_1}, r_{DD_2}, r_{DA}, \theta_{D_1DA}, \theta_{D_2DA}),$$

the total potential is obtained by

$$V = V_{AB} + V_{AC} + V_{AD} + V_{BA} + V_{CA} + V_{DA} \, . \tag{18}$$

The strain tensor and the curvature tensor are

$$\boldsymbol{U} = \begin{bmatrix} U_{11} & U_{12} & U_{13} \\ U_{21} & U_{22} & U_{23} \\ 0 & 0 & 1 \end{bmatrix}, \boldsymbol{K} = \begin{bmatrix} K_{11} & K_{12} & K_{13} \\ K_{21} & K_{22} & K_{23} \\ 0 & 0 & 0 \end{bmatrix} \, . \tag{19}$$

The components U_{13}, U_{23}, K_{13} and K_{23} contribute to the extra terms for shear energy and spin energy in the total energy formulation. Two principal directions $\boldsymbol{V}_I$ and $\boldsymbol{V}_{II}$ can be found on the reference plane. Let $\boldsymbol{A}_1$ and $\boldsymbol{A}_2$ be the components of the undeformed vector $\boldsymbol{A}$ along $\boldsymbol{V}_I$ and $\boldsymbol{V}_{II}$ directions, which then rotate to $\boldsymbol{A}_1$'and $\boldsymbol{A}_2$'by rotation tensors $\boldsymbol{R}_1$ and $\boldsymbol{R}_2$, as shown in Fig.3,

which defines the micro-rotation on the reference plane.

The principal curvatures $\boldsymbol{k}_I$ and $\boldsymbol{k}_{II}$ can be obtained from

$$\det\begin{bmatrix} K_{11}-k & K_{12} \\ K_{21} & K_{22}-k \end{bmatrix}=0 \quad . \tag{20}$$

The principal directions can be obtained from

$$\begin{bmatrix} K_{11}-k & K_{12} \\ K_{21} & K_{22}-k \end{bmatrix}\begin{Bmatrix} V_1 \\ V_2 \end{Bmatrix}=\begin{Bmatrix} 0 \\ 0 \end{Bmatrix} \quad . \tag{21}$$

The lattice vector $\boldsymbol{A}'$ is the vector that the undeformed lattice vector $\boldsymbol{A}$ rotates to after applying the rotation tensor, which is given by

$$\boldsymbol{A}'=\boldsymbol{R}_1(\boldsymbol{V}_I\cdot\boldsymbol{A})\boldsymbol{V}_I+\boldsymbol{R}_2(\boldsymbol{V}_{II}\cdot\boldsymbol{A})\boldsymbol{V}_{II} \quad . \tag{22}$$

The final deformed lattice vector $\boldsymbol{a}'$ is obtained after rotating by $\boldsymbol{R}$ then stretching by $\boldsymbol{U}$, which is expressed as

$$\boldsymbol{a}'=\boldsymbol{U}\boldsymbol{R}_1(\boldsymbol{V}_I\cdot\boldsymbol{A})\boldsymbol{V}_I+\boldsymbol{U}\boldsymbol{R}_2(\boldsymbol{V}_{II}\cdot\boldsymbol{A})\boldsymbol{V}_{II} \quad . \tag{23}$$

The bond length after deformation is

$$a=\sqrt{\boldsymbol{U}^T\boldsymbol{U}}A \quad . \tag{24}$$

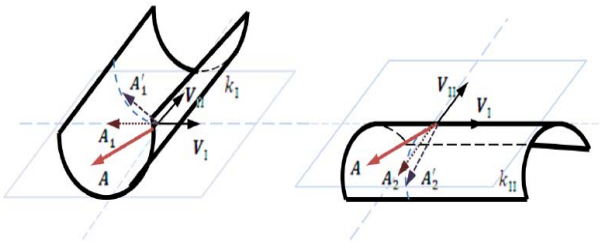

Fig. 3. Micro-rotation on the reference plane

The strain density is the total potential of the atom over the area it possesses

$$W_0(\boldsymbol{U},\boldsymbol{K},\boldsymbol{\eta})=\frac{V_{AB}+V_{AC}+V_{AD}+V_{BA}+V_{CA}+V_{DA}}{S_0}, \tag{25}$$

where $S_0=\left(3\sqrt{3}/2\right)A_0^2$. A_0 is the undeformed bond length. Considering the shift vector in Eq.(3), we have

$$\boldsymbol{r}_s=\boldsymbol{F}\left(\boldsymbol{r}_s^0+\boldsymbol{\eta}\right) \quad , \tag{26}$$

where the index s is a general term for all the bonds, for instance when s=AB, $\boldsymbol{r}_{AB}$ is the deformed lattice vector of A-B bond. Since the length doesn't change during the rotation, the deformed bond length only depends on the strain tensor $\boldsymbol{U}$

$$r_s(\boldsymbol{U},\boldsymbol{\eta})=\sqrt{\left(\boldsymbol{r}_s^0+\boldsymbol{\eta}\right)\boldsymbol{U}^T\boldsymbol{U}\left(\boldsymbol{r}_s^0+\boldsymbol{\eta}\right)} \quad , \tag{27}$$

where $\boldsymbol{r}_s^0$ is the undeformed bond vectors of the bond s. From Eq.(23), we have

$$\boldsymbol{r}_s=\boldsymbol{U}\boldsymbol{R}_1\left(\boldsymbol{V}_I\cdot\left(\boldsymbol{r}_s^0+\boldsymbol{\eta}\right)\right)\boldsymbol{V}_I+\boldsymbol{U}\boldsymbol{R}_2\left(\boldsymbol{V}_{II}\cdot\left(\boldsymbol{r}_s^0+\boldsymbol{\eta}\right)\right)\boldsymbol{V}_{II} \quad . \tag{28}$$

And the bond angles can be calculated from the deformed bond vectors, for example,

$$\theta_{BAC}=\arccos\frac{\boldsymbol{r}_{AB}\cdot\boldsymbol{r}_{AC}}{r_{AB}r_{AC}} \quad . \tag{29}$$

Define the bond lengths r_{AB}, r_{AC}, r_{AD}, r_{BB_1}, r_{BB_2}, r_{CC_1}, r_{CC_2}, r_{DD_1}, r_{DD_2} as a_i (i=1,2,…,9) and θ_{BAC}, θ_{BAD}, θ_{CAD}, θ_{B_1BA}, θ_{B_2BA}, θ_{C_1CA}, θ_{C_2CA}, θ_{D_1DA}, θ_{D_2DA} as θ_i (i=1,2,…,9). a_i and θ_i can be calculated in the potential form. The internal degree of freedom $\boldsymbol{\eta}$ can be determined by minimizing the strain energy density $W_0(\boldsymbol{U},\boldsymbol{K};\boldsymbol{\eta})$ with respect to $\boldsymbol{\eta}$

$$\frac{\partial W_0}{\partial\boldsymbol{\eta}}=0\Rightarrow\boldsymbol{\eta}=\boldsymbol{\eta}(\boldsymbol{U},\boldsymbol{K}). \tag{30}$$

The force tensor can be obtained from

$$\boldsymbol{S}=\frac{dW_0}{d\boldsymbol{U}}=\frac{\partial W_0}{\partial\boldsymbol{U}}+\frac{\partial W_0}{\partial\boldsymbol{\eta}}\frac{\partial\boldsymbol{\eta}}{\partial\boldsymbol{U}}=\frac{\partial W_0}{\partial\boldsymbol{U}}. \tag{31}$$

The couple tensor is

$$\boldsymbol{T}=\frac{dW_0}{d\boldsymbol{K}}=\frac{\partial W_0}{\partial\boldsymbol{K}}+\frac{\partial W_0}{\partial\boldsymbol{\eta}}\frac{\partial\boldsymbol{\eta}}{\partial\boldsymbol{K}}=\frac{\partial W_0}{\partial\boldsymbol{K}} \quad . \tag{32}$$

The tensor-like stretch modulus reads

$$\begin{aligned}\boldsymbol{n}&=\frac{d\boldsymbol{S}}{d\boldsymbol{U}}=\frac{\partial\boldsymbol{S}}{\partial\boldsymbol{U}}+\frac{\partial\boldsymbol{S}}{\partial\boldsymbol{\eta}}\frac{\partial\boldsymbol{\eta}}{\partial\boldsymbol{U}}=\frac{\partial^2W_0}{\partial\boldsymbol{U}\partial\boldsymbol{U}}+\frac{\partial^2W_0}{\partial\boldsymbol{U}\partial\boldsymbol{\eta}}\frac{\partial\boldsymbol{\eta}}{\partial\boldsymbol{U}}\\&=\frac{\partial^2W_0}{\partial\boldsymbol{U}\partial\boldsymbol{U}}-\frac{\partial^2W_0}{\partial\boldsymbol{U}\partial\boldsymbol{\eta}}\left(\frac{\partial^2W_0}{\partial\boldsymbol{\eta}\partial\boldsymbol{\eta}}\right)^{-1}\frac{\partial^2W_0}{\partial\boldsymbol{\eta}\partial\boldsymbol{U}}\end{aligned} \quad . \tag{33}$$

And the tensor-like bending modulus reads

$$\boldsymbol{m}=\frac{\partial^2W_0}{\partial\boldsymbol{K}\partial\boldsymbol{K}}-\frac{\partial^2W_0}{\partial\boldsymbol{K}\partial\boldsymbol{\eta}}\left(\frac{\partial^2W_0}{\partial\boldsymbol{\eta}\partial\boldsymbol{\eta}}\right)^{-1}\frac{\partial^2W_0}{\partial\boldsymbol{\eta}\partial\boldsymbol{K}}. \tag{34}$$

In the non-linear calculation, the minimizing of the strain energy density $W_0(\boldsymbol{U},\boldsymbol{K};\boldsymbol{\eta})$ with respect to $\boldsymbol{\eta}$ carries out by an updating procedure where the change of $\boldsymbol{\eta}$ is calculated by

$$\frac{\partial^2W_0}{\partial\boldsymbol{\eta}\partial\boldsymbol{\eta}}\Delta\boldsymbol{\eta}=-\frac{\partial W_0}{\partial\boldsymbol{\eta}}\Rightarrow\Delta\boldsymbol{\eta}=-\left(\frac{\partial^2W_0}{\partial\boldsymbol{\eta}\partial\boldsymbol{\eta}}\right)^{-1}\frac{\partial W_0}{\partial\boldsymbol{\eta}} \quad . \tag{35}$$

By inserting $\boldsymbol{\eta}$ into the potential, the stress fields and the modulus fields can be calculated via finite element iterations.

4 Results

A cylindrical shell model under stretch is designed as shown in Fig.4. Uniform stretching load is applied at both ends of the cylindrical shell. The length of the tube is fixed to L=8nm, the load at both ends is of a constant value of F=16nN, while the uniform load applied is p=16nN/b, with b being the width of sheet and $b=\pi D$, where D is the diameter of the tube, and u is the displacement. SWCNT's Young's modulus is calculated from the displacement u, through the relation

$$E = \frac{FL}{\pi Dhu} \quad . \tag{36}$$

First, an armchair SWCNT is studied and tube diameters are chosen from 0.407nm, increasing to 4.746nm, i.e. from (3,3) to (35,35) armchair SWCNTs. To provide results that can be compared with those of other authors, the effective wall thickness is chosen to be 0.34nm, as in [3,14-18]. The same method is applied to zigzag SWCNTs with length L=8nm, and F= 16nN. Accordingly, (6,0) to (60,0) zigzag SWCNTs are studied. The resulting values of Young's modulus for zigzag SWCNTs, as well as for armchair SWCNTs, are converging at 0.72TPa.

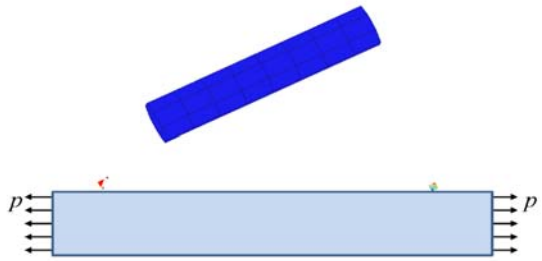

Fig. 4. Sketch of cylindrical shell model under tension

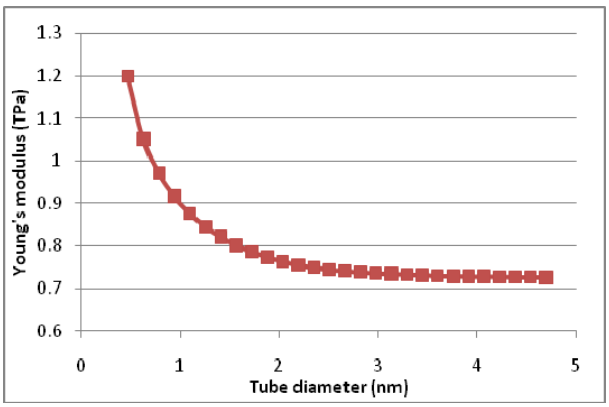

Fig. 5. Dependence of Young's modulus on tube diameter for zigzag SWCNTs

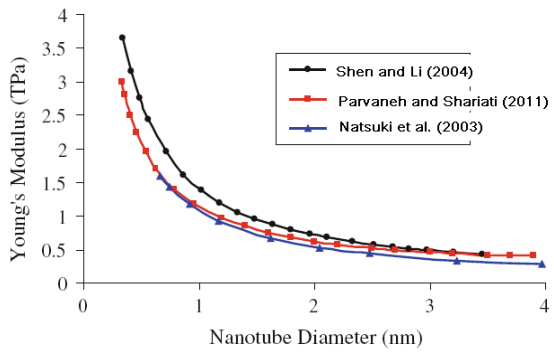

Fig. 6. Dependence of Young's modulus on tube diameter for zigzag SWCNTs [15]

[15] applied atomistic modelling through the use of ABAQUS, and produced results for Young's modulus of zigzag SWCNTs under axial tension, and compared it with two other authors, as shown in Fig.6. The results computed from the proposed approach, as shown in Fig.5, are in good agreement with the results from the literatures. [16] presented a molecular mechanics model to predict Young's modulus of SWCNTs. By comparing the Young's modulus for armchair and for zigzag SWCNTs, they obtained results with the same trend, as shown in Fig.8. Although they arrived at a minimum value of Young's modulus of ~1.04TPa, it showed that Young's modulus of zigzag SWCNTs is slightly larger than the one of armchair SWCNTs. The method proposed here provides comparable results, and the values become very close with increasing tube diameter, as shown in Fig.7.

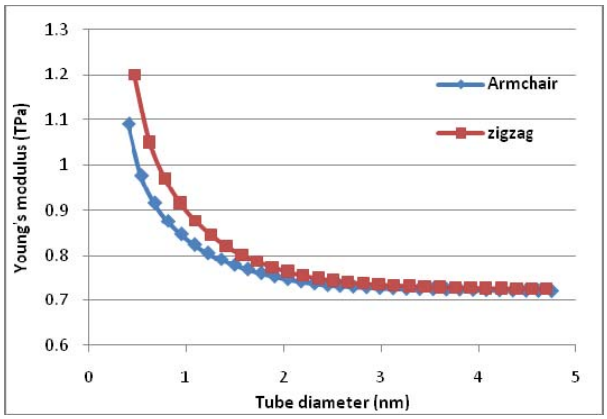

Fig. 7. Comparison of Young's modulus for armchair and zigzag SWCNTs

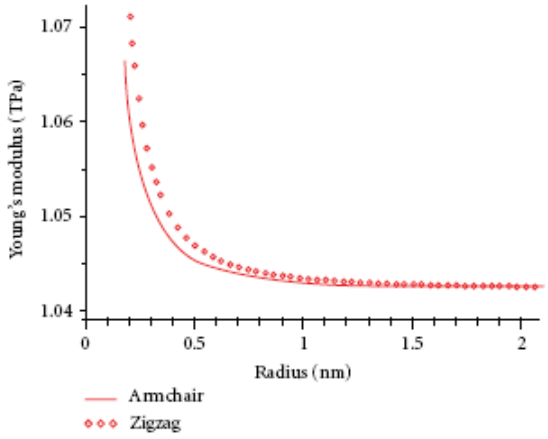

Fig. 8. Comparison of Young's modulus for armchair and zigzag SWCNTs [16]

5 Conclusion

This paper has presented an atomistic and continuum mixing approach to simulate SWCNT's

behavior, where the link between micro- and macro-space is by the standard Cauchy-Born rule. A Cosserat surface shell theory is adopted, where a rotation tensor is introduced to present a micro-rotation, which is independent from displacement field. SWCNT is modeled as a Cosserat surface, where the empirical atomistic potential forms are established based on the second generation REBO potentials. Force and modulus fields are derived from the derivatives of the potentials over the displacement and rotation fields. From the results of the Young's modulus, it is shown that, the Cosserat surface model is capable of providing comparable results with atomistic simulations, but with much lower computational overhead.

References:

[1] Iijima, S. Helical Microtubules of Graphitic Carbon. *Nature*, Vol.354, 1991, pp.56–58.

[2] Arroyo, M., Belytschko, T. Finite Element Methods for the Non-linear Mechanics of Crystalline Sheets and Nanotubes. *International Journal for Numerical Methods in Engineering*, Vol.59, 2004, pp.419-456.

[3] Guo, X., Wang, J. B., Zhang, H.W. Mechanical Properties of Single-walled Carbon Nanotubes Based on Higher Order Cauchy–Born Rule. *International Journal of Solids and Structures*, Vol.43, No.5, 2006, pp.1276-1290.

[4] Yang, J.Z., E, W. Generalized Cauchy-Born Rules for Elastic Deformation of Sheets, Plates, and Rods: Derivation of Continuum Models from Atomistic Models. *Physical Review B*, Vol.74, 2006, pp.4110-4127.

[5] Pantano, A., Parks, D. M., Boyce, M. C. Mechanics of Deformation of Single- and Multi-wall Carbon Nanotubes. *Journal of the Mechanics and Physics of Solids*, Vol.52, No.4, 2004, pp.789-821.

[6] Tu, Z., Ou-Yang, Z. Single-walled and Multiwalled Carbon Nanotubes Viewed as Elastic Tubes with the Effective Young's Moduli Dependent on Layer Number, *Physical Review B*, Vol.65, 2002, pp.3407-3430.

[7] Wu, J., Hwang, K.C., Song, J., Huang, Y. A Finite Deformation Shell Theory for Carbon Nanotubes Based on the Interatomic Potential—Part II: Instability Analysis. *Jounal of Applied Mechanics*, Vol.75, 2008, pp.1007-1012.

[8] Sansour, C., Bednarczyk, H. The Cosserat Surface as a Shell Model, Theory and Finite-element Formulation. *Computer Methods in Applied Mechanics and Engineering*, Vol.120, No.1-2, 1995, pp.1-32.

[9] Brenner, D.W. Tersoff-type Potentials for Carbon, Hydrogen and Oxygen. *Materials Research Society Symposium Proceedings*, Vol.141, 1989, pp.59-64.

[10] Liew, K.M., He, X.Q., Wong, C.H. On the Study of Elastic and Plastic Properties of Multi-walled Carbon Nanotubes Under Axial Tension Using Molecular Dynamics Simulation. *Acta Materialia*, Vol.52, No.9, 2004, pp.2521-2527.

[11] Bao, W.X., Zhu, C.C., Cui, W.Z. Simulation of Young's Modulus of Single-walled Carbon Nanotubes by Molecular Dynamics. *Physica B: Condensed Matter*, Vol.352, No.4, 2004, pp.156-163.

[12] Zhang, P., Huang, Y., Geubelle, P. H., Klein, P. A., Hwang, K. C. The Elastic Modulus of Single-wall Carbon Nanotubes: a Continuum Analysis Incorporating Interatomic Potentials. *International Journal of Solids and Structures*, Vol.39, No.13-14, 2002, pp.3893-3906.

[13] Brenner, D.W., Shenderova, O.A., Harrison, J.A., Stuart, S.J., Ni, B., Sinnott, S.B. A Second-generation Reactive Empirical Bond Order (REBO) Potential Energy Expression for Hydrocarbons. *Journal of Physics: Condensed Matter*, vol.14, 2002, pp.783–802.

[14] Avila, A.F., Lacerda, G.S. Molecular Mechanics Applied to Single-walled Carbon Nanotubes. *Materials Research*, Vol.11, No.3, 2008, pp.325-333.

[15] Parvaneh, V., Shariati, M. Effect of Defects and Loading on Prediction of Young's Modulus of SWCNTs. *Acta Mech*, Vol.216, 2011, pp.281–289.

[16] Lei, X., Natsuki, T., Shi, J. Ni, Q. Q. Analysis of Carbon Nanotubes on the Mechanical Properties at Atomic Scale. *Journal of Nanomaterials*, Vol.80, 2011, pp.5313-5322.

[17] Meo, M., Rossi, M. Prediction of Young's Modulus of Single Wall Carbon Nanotubes by Molecular-mechanics Based Finite Element Modelling. *Composites Science and Technology*, Vol.66, 2006, pp.1597–1605.

[18] Wang, J.B., Guo, X., Zhang, H.W., Wang, L., Liao, J.B. Energy and Mechanical Properties of Single-walled Carbon Nanotubes Predicted Using the Higher Order Cauchy-Born Rule. Physical Review B, Vol.73, No.11, 2006, pp.5428-5436.